

Acoustoelectric photoresponse in graphene

T. Poole, L. Bandhu, and G. R. Nash^{a)}

College of Engineering, Mathematics and Physical Sciences, University of Exeter, EX4 4QF Exeter, United Kingdom

(Received 16 February 2015; accepted 20 March 2015; published online 2 April 2015)

The acoustoelectric current in graphene has been investigated as a function of illumination, using blue (450 nm) and red (735 nm) light-emitting diodes (LEDs), and surface acoustic wave (SAW) intensity and frequency. The measured acoustoelectric current increases with illumination, more than the measured change in the conductivity of the graphene, whilst retaining a linear dependence on the SAW intensity. The latter is consistent with the interaction between the carriers and SAWs being described by a relatively simple classical relaxation model suggesting that the change in the acoustoelectric current is caused by the effect of the illumination on the electronic properties of the graphene. The increase in the acoustoelectric current is greatest under illumination with the blue LED, consistent with the creation of a hot electron distribution. © 2015 AIP Publishing LLC. [<http://dx.doi.org/10.1063/1.4916940>]

Graphene, an atomically-thin layer of carbon atoms arranged in a honeycomb lattice,^{1,2} naturally lends itself to integration with surface acoustic wave (SAW) devices, and over the last couple of years, there has been rapidly growing interest in this area. Theoretical studies predict a range of rich physical phenomena arising from SAW-graphene interactions,^{3–5} and graphene's potential as an extraordinarily responsive sensing material² is being exploited for the development of SAW sensors. For example, SAW devices have been reported that are responsive to hydrogen and carbon monoxide,⁶ and moisture.^{7,8} Huan *et al.*⁹ have very recently reported ZnO/glass humidity sensors with high sensitivity, exploiting a graphene oxide sensing layer, where the frequency response of the sensors was primarily caused by mass loading effects, which were also studied by Whitehead *et al.* in graphene-quartz SAW devices.¹⁰ Illumination of randomly stacked graphene flakes on lithium niobate (LiNbO₃) by 633 nm laser light¹¹ has been shown to modulate the SAW velocity, where this shift in the velocity was attributed to the increase in surface temperature resulting from optical energy absorbed in the graphene layer.

In conventional semiconductor two- (2D) and low-dimensional systems, the electric fields associated with SAWs travelling in a piezoelectric material have been further exploited, both as a contactless means of probing their electronic properties,^{12,13} and to trap and transport charge for applications such as metrology and quantum information processing.^{14–18} Acoustic charge transport has very recently been reported in graphene,^{19,20} and we have investigated it in monolayer graphene, produced by chemical vapour deposition (CVD), transferred onto lithium niobate SAW devices, both at room temperature²¹ and low temperature.²² In this paper, we show that illumination of the same devices, using blue (450 nm) and red (735 nm) light-emitting diodes (LEDs), causes an increase in the acoustoelectric current which is much larger than the associated change in the conductivity of the graphene. We believe that this is due to the

piezoelectric interaction between the SAWs and the hot carrier distribution created by the illumination.

Acoustic charge transport arises from the transfer of energy from the SAW to the carrier system, leading to a proportional loss of momentum,¹⁴ which appears as a force on the carrier system. In a closed circuit and in the absence of a magnetic field, the current density j as described by Rotter *et al.*¹⁴ and Fal'ko *et al.*¹⁵ reduces to

$$j = -\mu Q = -\mu \frac{I\Gamma}{v}, \quad (1)$$

where μ is the charge carrier mobility, Q is the phonon pressure given by $Q = I\Gamma/v$, I is the intensity of the SAW, Γ is the attenuation per unit length, and v is the SAW velocity in the piezoelectric (approximately 4000 ms^{-1} for LiNbO₃). The interaction between charged carriers in a 2D system and the piezoelectric fields associated with the SAW can often be described using a classical relaxation model, where the movement of the carriers to screen the SAW wavefronts causes attenuation due to Joule losses. In this model, the attenuation coefficient is given by

$$\Gamma = K^2 \frac{\pi}{\lambda} \left[\frac{\frac{\sigma}{\sigma_M}}{1 + \left(\frac{\sigma}{\sigma_M}\right)^2} \right], \quad (2)$$

where K^2 is the piezoelectric coupling coefficient (0.056 in LiNbO₃), λ is the SAW wavelength, σ is the conductivity of the graphene, and the attenuation has a maximum value for a characteristic conductivity σ_M . For a hybrid system based on LiNbO₃, $\sigma_M = v\epsilon_0(\sqrt{\epsilon_{xx}^S \epsilon_{zz}^S} + 1) = 1.25 \times 10^{-6} \Omega^{-1}$,¹⁴ where ϵ_0 is the permittivity of free space and ϵ_{xx}^S and ϵ_{zz}^S are the dielectric constants of LiNbO₃ at constant stress. The attenuation coefficient, and in turn the acoustoelectric current, is therefore predicted to have a non-monotonic dependence on the conductivity.

The layout of the samples used in these experiments is shown schematically in Figure 1. Commercially available

^{a)} Author to whom correspondence should be addressed. Electronic mail: g.r.nash@exeter.ac.uk

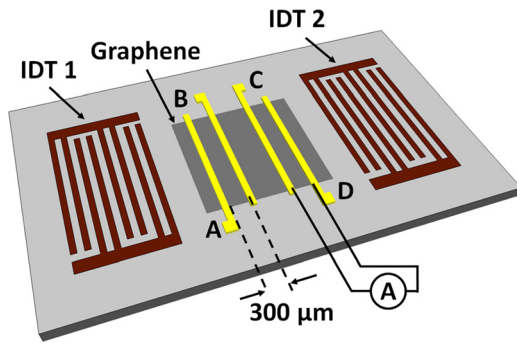


FIG. 1. Schematic diagram of the device layout. The SAW propagates from IDT 1 to IDT 2.

CVD graphene grown on copper (Graphene Supermarket) was positioned between the input and output interdigital transducers (IDTs) of a 128° YX LiNbO_3 SAW delay line using the PMMA transfer technique.²³ The IDTs were of a uniform, double-digit design with a 3.25 mm aperture. The acoustic path length was 5.2 mm, and the graphene's dimensions were 3 mm \times 3 mm. After transfer to the LiNbO_3 , Raman spectroscopy was used to confirm the monolayer nature of the graphene. Electron-beam lithography and thermal evaporation of 7 nm of Cr and 70 nm of Au were used to fabricate four large contacts (3 mm \times 20 μm) on top of the graphene. All measurements were performed between contacts C and D (Figure 1), separated by a distance of 300 μm . Full details of the device characterisation and fabrication are given in Ref. 21.

The device was bonded to a printed circuit board using a conductive, silver epoxy and then placed in a vacuum chamber with optical access. The chamber pressure was held at approximately 6×10^{-6} mbar, with continuous pumping to prevent the accumulation of dopants such as water.²⁴ Measurements of the acoustoelectric current were made using a Keithley K2400 source-measurement unit with no bias applied, whilst a Hewlett-Packard 8648C RF signal generator produced a continuous SAW at the input IDT. Measurements were made at SAW frequencies of 33 MHz and 355 MHz. Two-terminal current-voltage measurements in the absence of SAWs were used to determine the graphene's conductivity. The sample was exposed to light from either a Thorlabs MCWHL2 Cold White LED, or a Thorlabs red M735L2 LED, with their maximum emission at wavelengths of approximately 450 nm and 735 nm, respectively. A motorised shutter was used to allow or block illumination of the sample, and the emitted power from the LEDs was controlled by varying the drive current via a Thorlabs DC2100 driver.

In Figures 2(a) and 2(b), the acoustoelectric current is plotted as a function of time, at one second intervals, for SAW frequencies of 33 MHz and 355 MHz, respectively. In both cases, the output of the RF generator was set to +17.8 dBm. For the first hour of measurements, although the LED was on, the mechanical shutter was closed and prevented the device being illuminated. At both SAW frequencies, negative I_{ae} was observed, corresponding to the net transport of electrons by the SAW, suggesting that the sample was n-doped. This is in contrast to previous measurements²¹ where the acoustoelectric current corresponded to the net transport of holes. In the current case, the vacuum chamber, with the

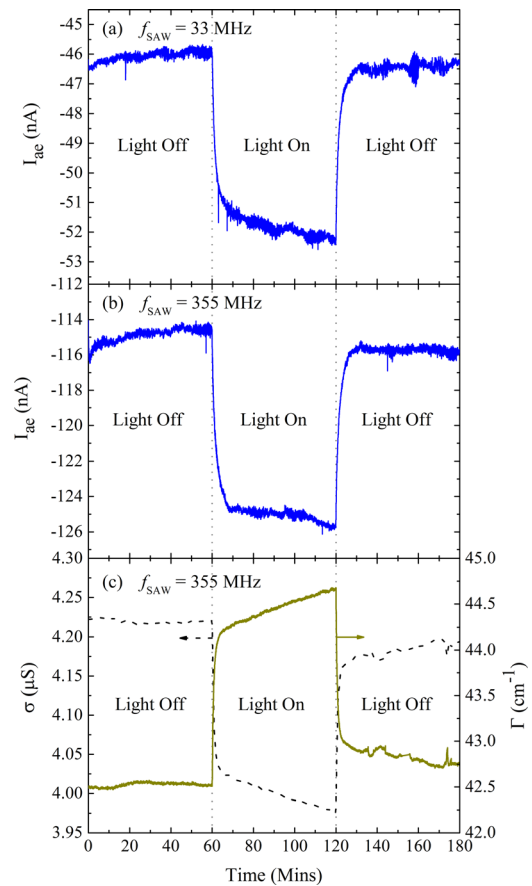


FIG. 2. Acoustoelectric current as a function of time at SAW frequencies of (a) 33 MHz and (b) 355 MHz, periodically illuminated by a Thorlabs MCWHL2 LED. (c) The sample conductivity recorded as a function of time (dashed line) is used to determine the attenuation coefficient (solid line) using Eq. (2).

sample mounted inside, was pumped continuously for a number of weeks before measurements began. During this period, the sign of the acoustoelectric current reversed, suggesting that the sample doping changed from p-type to n-type. At the same time, the measurements became noticeably more stable and reproducible.²⁵ This is illustrated in the data shown in Figures 2(a) and 2(b), where, during the period before illumination of the sample, the standard deviation/mean of the acoustoelectric current was approximately 0.34% for both $f_{\text{SAW}} = 33$ MHz and $f_{\text{SAW}} = 355$ MHz. After an hour, the shutter was opened and the sample was illuminated using the shorter wavelength LED with an incident intensity of approximately 0.84 mW mm⁻². At both SAW frequencies, there is a rapid increase in the measured I_{ae} on illumination, by 2.4% and 1.9%, respectively, within the first 20 seconds, after which the rate of change of acoustoelectric current decreased. The maximum change in I_{ae} measured at $f_{\text{SAW}} = 33$ MHz was 14%, compared to 10% at $f_{\text{SAW}} = 355$ MHz. The conductivity of the sample was also measured as a function of time over the same period as the measurements of I_{ae} , and is plotted in Figure 2(c) (dashed line). The increase in the acoustoelectric current under illumination is mirrored by a similar decrease of 6% in the conductivity. Note therefore that the measurement of acoustoelectric current is more sensitive to illumination than just a simple measurement of conductivity. After one hour of

illumination, the shutter was closed and the acoustoelectric current and conductivity rapidly decrease and increase, respectively, before approaching their values prior to illumination.

To determine whether the change in the measured acoustoelectric current is due to a change in the electronic properties of the graphene, where the attenuation of the SAW is given by the classical relaxation model described earlier, the acoustoelectric current is plotted as a function of SAW intensity at SAW frequencies of (a) 33 MHz and (b) 355 MHz in Figure 3. The lines shown are linear fits to the data, using Eq. (1), where we have calculated values of the attenuation coefficient from the measured conductivity. As expected from the classical relaxation model, the acoustoelectric current shows a near linear dependence on the SAW intensity, even under illumination (note that when the measured conductivity is much greater than the characteristic conductivity σ_M , as is the case for all the measurements presented here, the attenuation coefficient given in Eq. (2) becomes inversely proportional to the conductivity/mobility and values of the mobility cannot be directly extracted from the gradient of the straight line fits presented in Figure 3. The size of the measured acoustoelectric current is also larger for the higher frequency SAW, also consistent with the relaxation model, again suggesting that the change in the acoustoelectric current under illumination is due to a change in the electronic properties of the graphene.

To further probe the mechanism of the photoresponse of the acoustoelectric current, the experiments were repeated using illumination from the second LED (Thorlabs

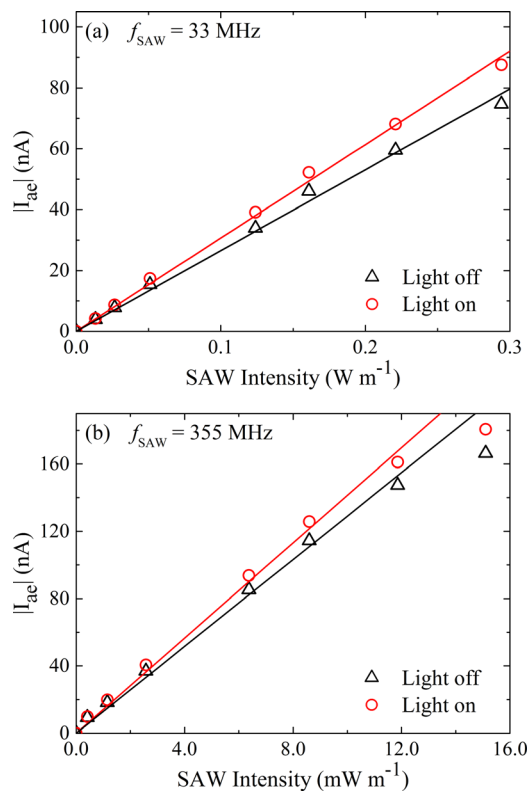


FIG. 3. Acoustoelectric current as a function of SAW intensity for SAW frequencies of (a) 33 MHz and (b) 355 MHz. Triangular points correspond to current measured when the sample was not illuminated; circular points show the case under illumination.

M735L2), which had its maximum emission at a longer wavelength of approximately 735 nm. In Figure 4, the change in the measured acoustoelectric current (before illumination-after illumination) is plotted as a function of incident optical power (corrected for the measurement geometry and emission characteristics of the LEDs), for the two LEDs at a SAW frequency of 33 MHz (very similar behaviour is observed at 355 MHz). The change in acoustoelectric current increases with the increase in intensity, for illumination under both LEDs, and exhibits a near-linear dependency (the dashed lines in Figure 4 are guides to the eye only) on the LED intensity. However, over most of the intensity range, the change in the acoustoelectric current due to illumination using the blue (450 nm) LED is much greater than that obtained under illumination with the red (735 nm) LED, and is approximately $3\times$ larger at an incident intensity of 0.8 mW mm^{-2} .

The observed dependence on photon energy (which is 1.7 eV and 2.8 eV for the red and blue LEDs respectively) is consistent with recent studies by Tielrooij *et al.*,²⁶ who used an ultrafast optical pump terahertz probe measurement technique to study the energy relaxation process of photoexcited electron-hole pairs in doped single-layer graphene. Using different pump photon energies, they were able to follow the ensuing energy relaxation dynamics and showed that carrier-carrier scattering is the dominant relaxation process, where energy is transferred to multiple secondary hot electrons in the conduction band, generating a hot carrier distribution. The number of secondary hot electrons increases with photon energy, leading to a hotter carrier distribution. In turn, this hot carrier distribution causes a decrease in the conductivity of the graphene,²⁷ due to a reduction in the mobility, which manifests itself in our measurements as a change in the measured acoustoelectric current. Finally, at low temperatures, the length scale over which the SAW probes the conductivity of the graphene (approximately one half of the SAW wavelength) was found to be important,²² reflecting, for example, the relative contribution to the conductivity of transport across the energy barriers associated with grain boundaries in the polycrystalline CVD graphene. However, in these measurements, the effect of illumination on the acoustoelectric current measured at SAW frequencies

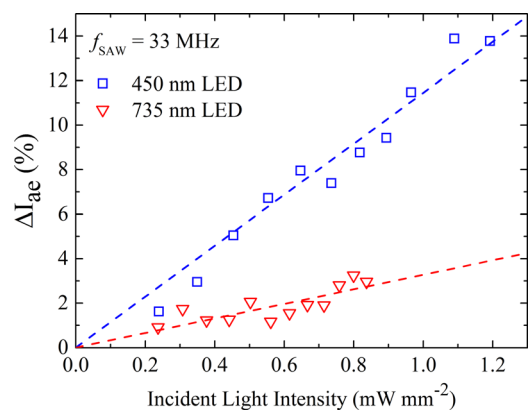


FIG. 4. The change in the measured acoustoelectric current caused by illumination with the blue and red LEDs at a SAW frequency of 33 MHz. The straight lines are guides to the eye only.

of 33 MHz and 355 MHz (corresponding to length scales of approximately 60 μm and 6 μm , respectively) is very similar, as might be expected if the conductivity of the graphene is dominated by a hot electron distribution.

In conclusion, we have investigated the acoustoelectric current in graphene as a function of illumination and surface acoustic wave (SAW) intensity and frequency. The measured acoustoelectric current increases with illumination, more than the measured decrease in the conductivity of the graphene, whilst retaining a linear dependence on the SAW intensity. The latter is consistent with the interaction between the carriers and SAWs being described by a relatively simple classical relaxation model, suggesting that the change in the acoustoelectric current is caused by the effect of the illumination on the electronic properties of the graphene. The change in the acoustoelectric current is also much greater under illumination with a blue (450 nm) LED compared to a red (735 nm) LED, consistent with the creation of a hot electron distribution. Very similar behavior was observed using SAW frequencies of 33 MHz and 355 MHz, which again is consistent with the conductivity of the graphene being dominated by hot carrier effects.

The authors would like to thank Gino Hrkac for useful discussions.

¹A. K. Geim and K. S. Novoselov, *Nat. Mater.* **6**, 183 (2007).

²K. S. Novoselov, V. I. Fal'ko, L. Colombo, P. R. Gellert, M. G. Schwab, and K. Kim, *Nature* **490**, 192 (2012).

³J. Schiefele, J. Pedrós, F. Sols, F. Calle, and F. Guinea, *Phys. Rev. Lett.* **111**, 237405 (2013).

⁴S. H. Zhang and W. Xu, *AIP Adv.* **1**, 022146 (2011).

⁵P. Thalmeier, B. Dóra, and K. Ziegler, *Phys. Rev. B* **81**, 041409 (2010).

⁶R. Arsath, M. Breedon, M. Shafiei, P. G. Spizziri, S. Gilje, R. B. Kaner, K. Kalanter-zadeh, and W. Wlodarski, *Chem. Phys. Lett.* **467**, 344 (2009).

⁷D. Čiplys, R. Rimeika, A. Sereika, V. Poderys, R. Rotomskis, and M. S. Shur, *Proceedings of the Nineth IEEE Sensors Conference*, Hawaii, IEEE Pub. No. CFP10SEN-PRT (IEEE, New York, 2010), pp. 787–788.

⁸Y. J. Guo, J. Zhang, C. Zhao, P. A. Hu, X. T. Zu, and Y. Q. Fu, *Optik* **125**, 5800 (2014).

⁹W. Xuan, M. He, N. Meng, X. He, W. Wang, J. Chen, T. Shi, T. Hasan, Z. Xu, Y. Xu, and J. K. Luo, *Sci. Rep.* **4**, 7206 (2014).

¹⁰E. F. Whitehead, E. M. Chick, L. Bandhu, L. M. Lawton, and G. R. Nash, *Appl. Phys. Lett.* **103**, 063110 (2013).

¹¹V. S. Chivukula, D. Čiplys, J. H. Kim, R. Rimeika, J. M. Xu, and M. S. Shur, *IEEE Trans. Ultrason., Ferroelectr., Freq. Control* **59**, 265 (2012).

¹²A. Wixforth, J. Scriba, M. Wassermeier, J. P. Kotthaus, G. Weimann, and W. Schlapp, *Phys. Rev. B* **40**, 7874 (1989).

¹³See, for example, G. R. Nash, S. J. Bending, M. Boero, P. Grambow, K. Eberl, and Y. Kershaw, *Phys. Rev. B* **54**, R8337 (1996).

¹⁴M. Rotter, A. Wixforth, W. Ruile, D. Bernklau, and H. Riechert, *Appl. Phys. Lett.* **73**, 2128 (1998).

¹⁵V. I. Fal'ko, S. V. Meshkov, and S. V. Iordanskii, *Phys. Rev. B* **47**, 9910 (1993).

¹⁶J. M. Shilton, D. R. Mace, V. I. Talyanskii, Y. Galperin, M. Y. Simmons, M. Pepper, and D. A. Ritchie, *J. Phys.: Condens. Matter* **8**, L337 (1996).

¹⁷O. D. Couto, Jr., S. Lazić, F. Iikawa, J. A. H. Stotz, U. Jahn, R. Hey, and P. V. Santos, *Nature Photonics* **3**, 645 (2009).

¹⁸S. Hermelin, S. Takada, M. Yamamoto, S. Tarucha, A. D. Wieck, L. Saminadayar, C. Bauerle, and T. Meunier, *Nature* **477**, 435 (2011).

¹⁹V. Miseikis, J. E. Cunningham, K. Saeed, R. O'Rourke, and A. G. Davies, *Appl. Phys. Lett.* **100**, 133105 (2012).

²⁰P. V. Santos, T. Schumann, M. H. Oliveira, J. M. J. Lopes, and H. Riechert, *Appl. Phys. Lett.* **102**, 221907 (2013).

²¹L. Bandhu, L. M. Lawton, and G. R. Nash, *Appl. Phys. Lett.* **103**, 133101 (2013).

²²L. Bandhu and G. R. Nash, *Appl. Phys. Lett.* **105**, 263106 (2014).

²³X. Li, W. Cai, J. An, S. Kim, J. Nah, D. Yang, R. Piner, A. Velamakanni, I. Jung, E. Tutuc, S. K. Banerjee, L. Colombo, and R. S. Ruoff, *Science* **324**, 1312 (2009).

²⁴T. O. Wehling, A. I. Lichtenstein, and M. I. Katsnelson, *Appl. Phys. Lett.* **93**, 202110 (2008).

²⁵T. Poole, L. Bandhu, and G. R. Nash, "Photoresponse of Acoustoelectric Effect in Graphene," (unpublished).

²⁶K. J. Tielrooij, J. C. W. Song, S. A. Jensen, A. Centeno, A. Pesquera, A. Zurutuza Elorza, M. Bonn, L. S. Levitov, and F. H. L. Koppens, *Nat. Phys.* **9**, 248 (2013).

²⁷F. H. L. Koppens, T. Mueller, Ph. Avouris, A. C. Ferrari, M. S. Vitiello, and M. Polini, *Nat. Nanotechnol.* **9**, 780 (2014).